Contrast echocardiography for pulmonary blood volume quantification

Contrast Echocardiography for Pulmonary Blood Volume Quantification

Massimo Mischi, Ton A. Kalker, *Fellow, IEEE*, and Erik H. Korsten

***Abstract*—Pulmonary blood volume quantification is important both for diagnosis and for monitoring of the circulatory system. It requires employment of transpulmonary indicator dilution techniques, which are very invasive due to the need for double catheterization. This paper presents a new minimally invasive technique for blood volume quantification. An ultrasound contrast agent bolus is injected peripherally and detected by an ultrasound transducer in the central circulation. Several echocardiographic views permit simultaneous detection of contrast in different cardiac cavities and central vessels, and acoustic backscatter measurements produce multiple indicator dilution curves (IDCs). Contrast mean-transit-time differences are derived from the IDC analysis and multiplied times cardiac output for the assessment of blood volumes between different detection sites. For pulmonary blood volume estimates, the right ventricle and the left atrium IDCs are measured. The mean transit time of the IDC is estimated by specific modelling. The Local Density Random Walk and the First Passage Time models were tested for IDC interpolation and interpretation. The system was validated *in vitro* for a wide range of flows. The results show very accurate volume measurements. The volume estimate determination coefficient is greater than 0.999 for both model fits. A preliminary study in patients shows promising results.**

I. Introduction

Blood volume measurements provide valuable information on circulatory system functionality. In particular, the pulmonary blood volume (PBV, blood volume between the pulmonary artery and the left atrium) and the central blood volume (CBV, blood volume between the pulmonary artery and the aortic valve) are important parameters in both anesthesiology and cardiology to evaluate cardiac preload and the symmetry of cardiac efficiency. For instance, left ventricular ejection fraction and stroke volume are related to PBV and CBV [1] [2]. The PBV measurements are based on transpulmonary indicator dilution techniques, which are based on the injection and subsequent detection of an indicator bolus [3]–[5]. The indicator concentration-versus-time curve is referred to as the indicator dilution curve (IDC), and contains the information for the volume measurement.

Nowadays, transpulmonary indicator dilution techniques are very invasive due to the need for a double catheterization [1], [2], [6]–[9]. In fact, a catheter for thermodilution (or dye dilution) must be inserted through the femoral artery up to the aorta, where the IDC is measured. Moreover, since the indicator must be injected into a central vein, the insertion of a second catheter is necessary to reach the injection site. The mean transit time (MTT) that the indicator takes to cover the distance between the injection site (central vein) and the detection site (aorta out-track) is multiplied times the cardiac output (CO, blood flow through the heart [10]). The result is the blood volume between the two sites, i.e., the PBV plus the average volume of the four cardiac chambers, which is referred to as intrathoracic blood volume. If the injection is performed in the pulmonary artery, the estimated volume is the CBV.

This paper presents a new non-invasive approach that uses an ultrasound contrast agent (UCA) as an indicator for the dilution method. UCAs are micro-bubbles (diameter from 1 to 10 μm) of gas stabilized by a shell of biocompatible material and easily detectable by ultrasound investigation [11]–[18]. They are injected into a peripheral vein and detected in the central circulation by a transthoracic ultrasound transducer. The video or acoustic intensity is measured in different regions of interest (ROI) in the B-mode output [19] of an ultrasound scanner in order to derive different IDCs.

For very small UCA doses (bolus of 0.25 mg of SonoVue®(Bracco Diagnostics, Milan, Italy) diluted in 5 mL of saline [18], [20]) and low ultrasound mechanical index[1] (MI = 0.1), the relation between UCA concentration and acoustic intensity is linear and the relation between UCA concentration and video intensity can be easily modelled [14], [15], [17], [21], [22]. In fact, for such a small dose of contrast, signal saturation due to attenuation is neglectable.

The UCA IDC measurements are influenced by several noise sources, such as bad mixing of the contrast, acoustic reverberation, backscatter oscillations due to pressure variations and respiration, bubble disruption due to ultrasound pressure, blood-acceleration artifacts, and contrast recirculation, resulting in very noisy IDCs. An accurate characterization and filtering of all the noise components is very complex; therefore, the employment of an IDC model is necessary for signal interpolation and interpretation.

Several models have been used for the IDC fitting; however, we focus on the Local Density Random Walk

Manuscript received December 19, 2003; accepted April 16. 2004.

The authors are with the Eindhoven University of Technology, Eindhoven, The Netherlands (e-mail: m.mischi@tue.nl).

E. H. Korsten is also with Catharina Hospital Eindhoven, The Netherlands.

[1]Ratio between the peak rarefactional pressure expressed in MPa and the square root of the central frequency of the ultrasound pulse expressed in MHz.

(LDRW) model and the First Passage Time (FPT) model, since they give an excellent fit and interpretation of the IDC [3], [4], [23]–[28]. Both models represent the contrast injection by means of an impulse function (Dirac function). The injected contrast flows through a fluid-dynamic system (an infinitely-long tube) and is detected in a different site.

The difference between the models concerns the bubble passage through the detection site. The FPT model hypothesis allows only a single passage of the bubbles, whereas the LDRW model hypothesis includes multiple passages. In the UCA dilution context, a practical hypothesis is a compromise between the FPT and the LDRW models. In fact, despite the use of a small MI, some of the bubbles are still destroyed while passing through the ultrasound pressure beam. Therefore, both models are tested for the UCA IDC interpretation.

The LDRW model assumes a Gaussian spatial distribution of the contrast that translates (convection) with the same velocity of the carrier fluid, and spreads (diffusion) with a variance that is a linear function of time t. The IDC at the detection site is reported by several authors [24]–[28] as given in (1), where m is the injected dose of contrast, Q is the (volumetric) flow of the carrier fluid, μ is the time to cover the distance between injection and detection sites at the carrier fluid velocity, and λ represents the skewness of the curve and is equal to Pe/2, where Pe is the Peclet number and represents the ratio between diffusion and convection of a tracer in a hydrodynamic system.

$$C(t) = \frac{m}{Q}\, e^{\lambda} \sqrt{\frac{\lambda}{2\pi\mu t}}\, e^{-\frac{\lambda}{2}\left(\frac{t}{\mu}+\frac{\mu}{t}\right)} \tag{1}$$

Although the LDRW model is a statistical model, it is also related to the physics of the dispersion process. In fact, it can also be derived by solving the drifting diffusion equation with infinite tube boundary conditions [3], [22].

The FPT model is derived from the LDRW model (see Appendix) when only the first passage through the detection site is considered. The FPT model formulation [25]–[27] is given in (2), where the meaning of the symbols is the same as for (1).

$$C(t) = \frac{m}{Q}\, e^{\lambda} \sqrt{\frac{\lambda\mu}{2\pi t^3}}\, e^{-\frac{\lambda}{2}\left(\frac{t}{\mu}+\frac{\mu}{t}\right)} \tag{2}$$

Fig. 1 shows three different LDRW and FPT curves for different values of λ.

The product of the contrast MTT and the carrier fluid flow (CO in the circulatory system) equals the volume between the injection and detection sites [29], [30]. The MTT is directly derived from both the fitted models and is equal to the parameter μ. Also, the flow, according to the Stewart-Hamilton equation[2] [5], [10], can be derived from the fitted model and is equal to the parameter Q [22]. However, even when the system is not calibrated for flow measurements, i.e., the linear relation between acoustic intensity and contrast concentration is not quantified, aortic echo-Doppler time integration can be adopted for non-invasive CO assessments [31].

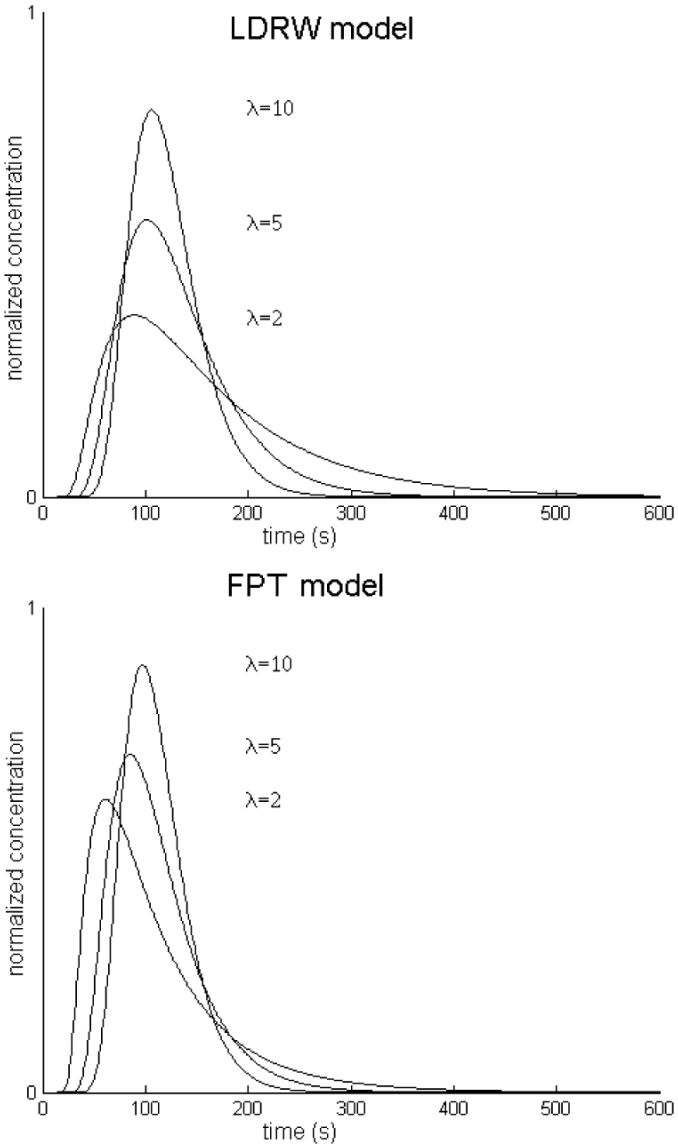

Fig. 1. LDRW and FPT models for λ equal to 2, 5, and 10. μ is fixed and equal to 100 s.

A specific algorithm has been developed for the LDRW model IDC fitting [22]. It is based on a least squares linear regression to the IDC logarithm, which is combined with an iterative search for the injection time. The same fitting strategy is adapted and implemented for the FPT model fitting.

The application of the UCA dilution technique for volume measurements requires the use of specific echocardiographic views. In fact, some of them permit IDC measurements in all four cardiac chambers as well as the central vessels, leading to a non-invasive assessment of the blood volume between the measurement sites. Contrast MTTs are estimated in different sites by IDC model fitting, and blood volumes are assessed as the product between MTT

[2]The Stewart-Hamilton equation states that the flow equals the injected dose (g) divided by the IDC integral (g·s/L).

differences and CO. As a result, different volumes, such as the pulmonary, the intrathoracic, the central, and the systemic blood volumes, can be measured with minimal invasiveness [30]. The PBV assessment requires the positioning of two ROIs in the right ventricle and the left atrium.

For the *in vitro* validation of the system, SonoVue IDCs were detected by a Sonos 5500 ultrasound scanner (Philips Medical Systems, Best, The Netherlands). For a better contrast detection, the scanner was set in power modulation mode. Both the LDRW and the FPT models were employed for the measurements. The results showed very accurate volume measurements using both models. The standard deviation of the volume estimates was always smaller than 3.2% in a range of flows from 1 to 5 L/min. The determination coefficient between real and estimated volumes was larger than 0.999 with both models. The *in vivo* application of the system was tested on a group of seven patients: six heart failure patients (bioventricular pacing candidates) and one patient before undergoing pneumonectomy.

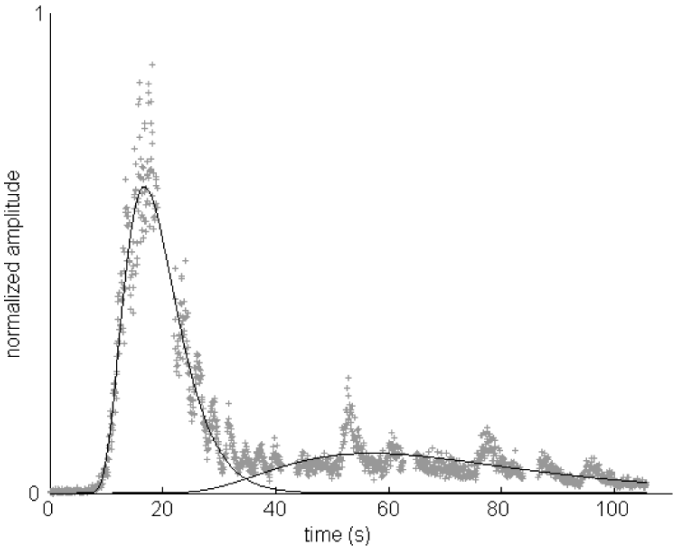

Fig. 2. Example of right ventricle IDC. The recirculation of the contrast generates a second rise of the IDC, which covers the tail of the first passage IDC. The LDRW model curve fit is shown, too. It allows extracting the first passage IDC and even defining the second passage IDC, which is due to the recirculation.

II. Methodology

A. Modelling

The volume measurement system is based on the detection in different sites of an injected UCA bolus. The injected contrast is detected by an ultrasound transducer and the acoustic intensity measured. For small UCA doses, the backscattered acoustic intensity is linearly related to the contrast concentration, so that the normalized acoustic intensity curve can be directly interpreted as a normalized IDC (Fig. 2). As a result, several parameters, including the PBV, can be measured with minimal invasiveness. Unfortunately, the contrast concentration measurements are influenced by several noise sources, resulting in low signal-to-noise ratio (SNR) IDCs.

The contrast recirculation in a closed system represents the major noise component. Only the first passage IDC contains the information for the parameter measurements; therefore, it must be extracted from the signal that is generated by the subsequent contrast passages (recirculation, see Fig. 2). The analysis of an IDC with contrast recirculation requires the employment of specific modelling techniques. A model is fitted to the first part of the IDC in order to derive the second part, which is masked by the recirculation signal.

The models adopted for IDC interpretation are the LDRW model and the FPT model. The LDRW model is based on the assumption of Brownian motion of the contrast bubbles, which follow a random walk trajectory. It is a statistical interpretation of the dispersion process and a solution of the drifting diffusion equation. The derivation of the LDRW model is reported in the literature [3], [4], [22], [24]. The FPT model derivation is very complex; however, it can be derived from the LDRW model when an absorber layer is placed right after the detection site (see Appendix). As a consequence, only a single passage of the bubbles is allowed.

The LDRW IDC fitting is performed by a specific algorithm [22]. The logarithm of the IDC is fitted by a multiple linear regression technique. The injection time is automatically determined by an iterative least squares search. The same algorithm is adapted for the FPT model fitting.

B. Volume Measurements and Contrast Mean Transit Time

The infinite tube model, as for the derivation of the LDRW and the FPT models, is adopted to derive a formula for the volume measurement. A carrier fluid flows through the tube with a steady flow Q. An indicator bolus is injected (fast injection) at time $t = 0$ into the tube. The volume to measure is defined as the tube segment between the indicator injection and detection sections.

We define $f(t)dt$ as the fraction of injected indicator that leaves the tube segment in the time interval $[t, t+dt]$. It is assumed that the indicator may not pass more than once through the detection section (FPT model hypothesis).

Due to the single passage hypothesis, the fraction of bubbles leaving corresponds to the fraction of bubbles that appear at the detection section. Therefore, $f(t)$ equals the normalized indicator concentration that is measured at the detection site and is given as in (3).

$$f(t) = \frac{C(t)}{\int_0^\infty C(\tau)d\tau} \tag{3}$$

The fraction of indicator that has left the segment by time t is determined by $F(t)$ as in (4).

$$F(t) = \int_0^t f(\tau)d\tau \tag{4}$$

The volume of fluid that enters the tube segment in the time interval $[0, dt]$ is $Q \cdot dt$ and the fraction that leaves the segment by time t is $Q \cdot dt \cdot F(t)$. Therefore, the volume of fluid that enters and leaves the tube segment in the time interval $[0, t]$ is given as in (5).

$$Q \int_0^t F(\tau)d\tau \tag{5}$$

The difference between the entering and the leaving fluid volumes in the time interval $[0, t]$ is then given as in (6).

$$Qt - Q \int_0^t F(\tau)d\tau \tag{6}$$

Therefore, (6) expresses the volume of fluid that enters the segment in the time interval $[0, t]$ and is still in the segment at time t. For time $t \to \infty$, all the fluid in the segment is replaced by fluid that has entered for $t \geq 0$. Therefore, the total volume V of the segment is given as in (7).

$$V = \lim_{t\to\infty} Q \left(t - \int_0^t F(\tau)d\tau \right) \tag{7}$$

Eq. (7) can be also formulated[3] as given in (8).

$$V = \lim_{t\to\infty} Q \left[t - [\tau F(\tau)]_0^t + \int_0^t \tau f(\tau)d\tau \right] = Q \int_0^\infty \tau f(\tau)d\tau \tag{8}$$

Due to the definition of $f(t)$ and the FPT hypothesis, the right term of (8) represents the multiplication of the flow Q times the MTT of the indicator, i.e., the average time that the indicator takes to cover the distance between the injection and the detection sections. Moreover, due to the FPT hypothesis and (3), $f(t)$ may be represented by (2) (except for the coefficient m/Q), which proves the convergence of the integral in (7).

[3]The integration per parts of $\int_0^t \tau f(\tau)d\tau$ allows replacing $\int_0^t F(\tau)d\tau$ in (7). In fact, $\int_0^t \tau f(\tau)d\tau = \int_0^t \tau dF(\tau) = [\tau F(\tau)]_0^t - \int_0^t F(\tau)d\tau$.

In conclusion, the volume is given as in (9), where the MTT of the indicator, which equals the first moment of the IDC, is given as in (10).

$$V = Q \cdot MTT \tag{9}$$

$$MTT = \int_0^\infty \tau f(\tau)d\tau = \frac{\int_0^\infty \tau C(\tau)d\tau}{\int_0^\infty C(\tau)d\tau} \tag{10}$$

The definition of the indicator MTT as the first moment of the IDC is appropriate only under the single-passage hypothesis. In this case, the MTT corresponds to the mean residence time (MRT) of the indicator in the defined segment and equals μ in (2), [25], [29], [30]. In fact, the bubble appearance time at the detection section also corresponds to the disappearance time from the segment.

The LDRW model is more general and does not satisfy the hypothesis of single passage of the indicator. As a consequence, the first moment of the model, which still represents the MRT of the indicator in the tube segment [3], [24], differs from the MTT. The MTT, which is defined as the average time that the indicator takes to go from the injection to the detection site, is equal by definition to μ in (1). In fact, in the LDRW model, μ equals the time that elapses to cover the distance between the injection and detection sites at the carrier fluid velocity, i.e., the MTT of the indicator. Instead, the first moment of the model, which corresponds to the MRT, equals $\mu(1 + 1/\lambda)$ [24]. Therefore, the MRT exceeds the MTT by the term $\mu/\lambda = 2D/u^2$, i.e., twice the ratio between indicator diffusion constant D (see Appendix) and squared velocity of the carrier fluid u^2 [3]. Large diffusion constants lead to increased numbers of bubble passages through the detection site and, therefore, to large differences between MRT and MTT.

In conclusion, when either the LDRW model or the FPT model is fitted to the IDC, (9) corresponds to (11).

$$V = Q \cdot \mu \tag{11}$$

Several techniques may be employed for the assessment of the flow Q [10], [32].

C. Deconvolution and Impulse Response

The fluid-dynamic dilution system between contrast injection and detection is a linear system. In fact, if two boluses of mass equal to αm and βm are injected ($\alpha, \beta \in \mathsf{R}$), the detected IDC, as from (1) or (2), equals $\alpha C(t) + \beta C(t)$. As a consequence, the system can be described by an impulse response and both the models given in (1) and (2) can be considered as the system impulse response.

Since both models assume an ideal bolus injection, which is modelled as a Dirac function and differs from a real injection, a deconvolution technique is adopted to estimate the impulse response of the dilution system [33], [34]. Due to small SNR, direct deconvolution techniques fail.

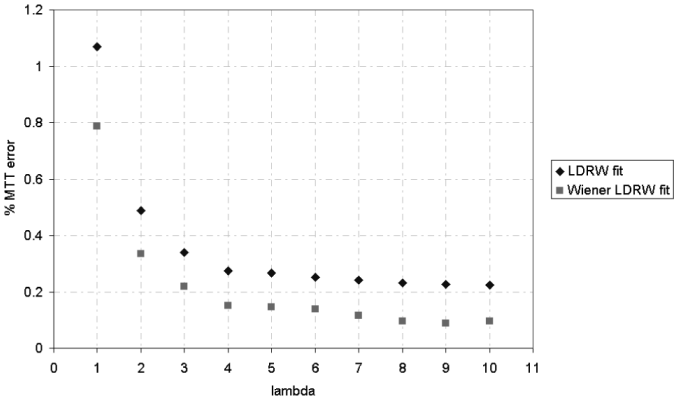

Fig. 3. Wiener filter validation results. LDRW curves are generated and convoluted with a rectangle (injection function) of 0.8 s. White noise is added to the curve and the SNR is reduced to 20 dB. 1000 different noise sequences are used and 1000 different IDCs generated for each integer value of $\lambda \in [1, 10]$. MTTs are estimated with and without Wiener filtering, and the average MTT-estimate percent error is calculated.

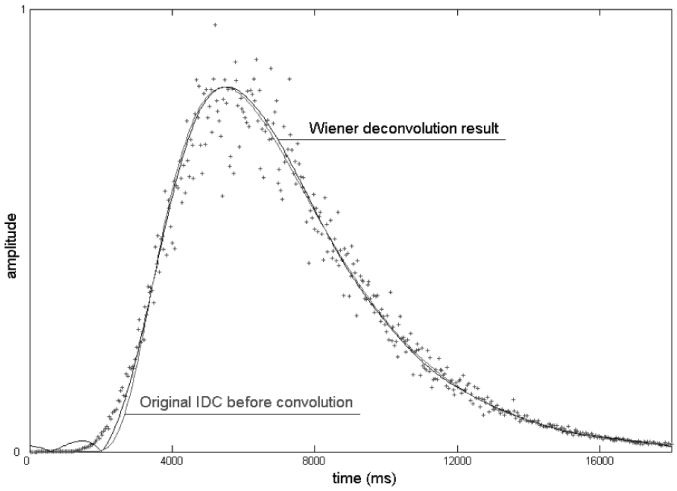

Fig. 4. Example of IDC simulation for Wiener filter validation. The plus-points represent the convoluted noisy IDC, which is deconvoluted to estimate the original IDC.

A possible solution is the employment of least squares techniques, such as Wiener deconvolution filtering [35], [36]. The Wiener filter $W(\omega)$ is designed in the frequency domain with the hypothesis of uncorrelated noise as given in (12). The R^* term is the complex conjugated Fourier transformation of a real injection function, which is represented by a 0.8-s rectangular input, and S_{rr}, S_{hh}, and S_{nn} are the injection function, the impulse response, and the noise power spectrum, respectively.

$$W(\omega) = \frac{R^*}{S_{rr} + \dfrac{S_{nn}}{S_{hh}}} \tag{12}$$

The S_{hh} term is estimated as the spectrum of the IDC model fit (without deconvolution) while S_{nn} is estimated as the spectrum of the difference between the IDC and the fitted model. The measured IDC is filtered by the Wiener filter in (12) to obtain the impulse response of the system between injection and detection. The resulting impulse response estimate is fitted and interpreted by the models for the parameter assessment.

The Wiener filter is tested by a specific simulation. A LDRW curve is generated and convoluted with a rectangular injection function of 0.8 s. The SNR is then reduced by white noise addition [22]. As for real UCA IDCs, the generated noise amplitude is linearly related to the signal amplitude [22]. The simulated IDC is then filtered by the Wiener filter and fitted by the LDRW model. For each integer value of $\lambda \in [1, 10]$, a set of 1000 IDCs is generated with SNR = 20 dB (noise-to-signal amplitude ratio equal to 0.1), which is a typical ratio for real signals. The range of values for the parameter λ covers and exceeds the values encountered in clinical practice.

The fitting results in terms of average percentage MTT-estimate (μ) error are shown in Fig. 3. We may conclude that the use of deconvolution filtering leads to more accurate MTT estimates. The standard deviation of the estimates equals 0.38% with and without Wiener deconvolution. Fig. 4 shows a simulation example for SNR = 20 dB and injection function R equal to a rectangle of 2 s.

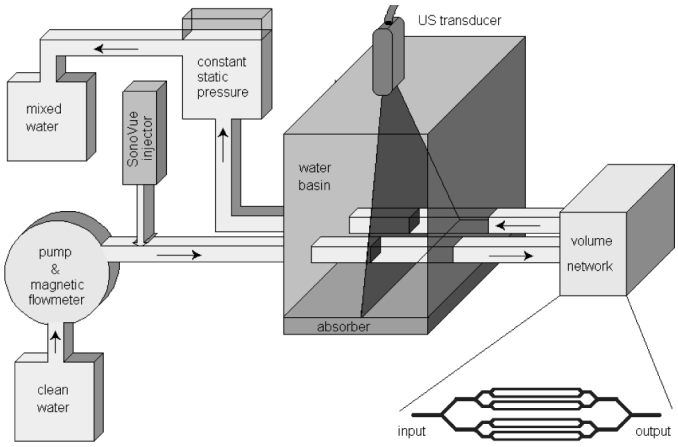

Fig. 5. *In vitro* set-up for volume measurements.

D. Validation Set-up

The measurement of blood volumes by means of UCA dilution was tested and validated *in vitro*. A specific hydrodynamic system was built to produce different water volumes as shown in Fig. 5. The system consists of a flow generator (a calibrated Medtronic 550 (Medtronic, Minneapolis, MN) bio-console centrifugal pump), a measurement water-filled basin, a tube network that simulates the PBV, and a pressure stabilizer. The generated flow, which is controlled by an electromagnetic flowmeter, passes the water-filled basin through a very thin polyurethane tube. After the basin, the tube expands into a network of eight tubes and converges again into a single tube that passes back through the basin. The hydrodynamic circuit is open in order to avoid UCA recirculation and the output static pressure is stabilized. The ultrasound measurements are per-

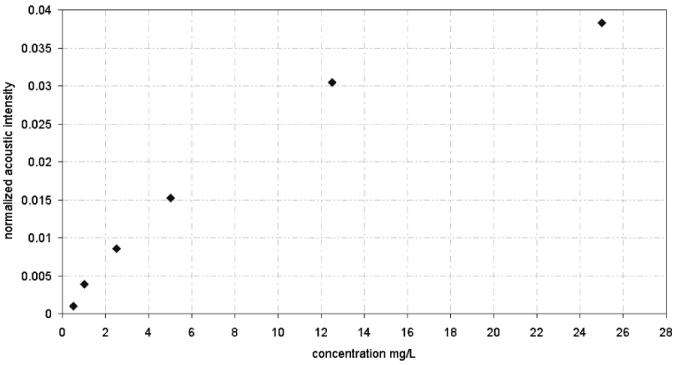

Fig. 6. Acoustic intensity calibration curve for the power modulation mode using a Sonos 5500 ultrasound scanner. The backscattered acoustic intensity is measured for SonoVue concentrations ranging from 0.5 to 25 mg/L.

formed in the basin. An ultrasound transducer is mounted on the basin, so that both the tubes are simultaneously insonated. The transducer, a Philips S3 probe, is fixed for stability and submerged to optimize acoustic impedance matching. It is covered by conductive gel and isolated from water by a thin plastic layer. The bottom of the basin is covered by an absorbing layer to reduce acoustic reverberation.

A Sonos 5500 ultrasound scanner is used to generate B-mode videos. The scanner is set in Tissue Contrast Enhancement mode at 25 frames per second and the MI is fixed to 0.1. Series of three adjacent ultrasound pulses of four cycles at 1.9 MHz are transmitted. The amplitude of the central pulse is twice that of the side pulses. The receiver sums the reflections of the side pulses and subtracts the reflection of the central pulse. This technique, which is a specific implementation of the power modulation mode, allows the enhancement of the bubble nonlinear response and the cancellation of the tissue linear response. For low contrast concentrations, this harmonic imaging setting shows a very high correlation coefficient between contrast concentration and backscattered acoustic intensity.

Fig. 6 shows the detected acoustic intensity using the described harmonic setting and concentrations of SonoVue varying from 0.5 to 25 mg/L. Above 12.5 mg/L the attenuation effect becomes evident. Below this threshold, the correlation coefficient between concentration and acoustic intensity is 0.99 and the relation is well approximated by a linear function. For equal transmitted intensity, the use of specific contrast modes allows reduction of the injected dose of contrast with a consequent improvement of the linear relation between contrast concentration and backscattered acoustic intensity.

A small bolus of UCA is injected right after the pump to minimize disruption of bubbles. The bolus consists of 5 mL of SonoVue diluted 1:100 in saline (sodium chloride 0.9%), which corresponds to 0.25 mg of SonoVue. With this dose, the threshold of 12.5 mg/L is never surpassed. As a consequence, the attenuation effect is neglectable and the relation between UCA concentration and backscattered acoustic intensity is linear [17], [22]. The passage of the contrast bolus through the first tube (before the network) and the second tube (after the network) is recorded by the ultrasound scanner. The B-mode digital records are analyzed by the software Q-Lab®(Philips Medical Systems, Best, The Netherlands), especially designed for acoustic quantification of digital data generated by Sonos ultrasound scanners.

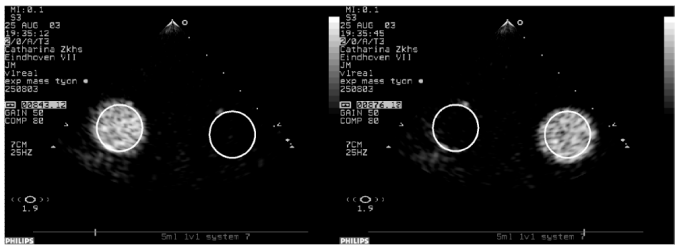

Fig. 7. Two B-mode frames showing the passage of the contrast bolus through the first tube (left frame) and the second tube (right frame). A ROI is placed on each tube for the IDC measurements.

A ROI is overlapped on each tube to quantify the acoustic intensity that is backscattered by the contrast passage (Fig. 7). Therefore, two IDCs (one for each tube) are generated. The IDCs are processed and fitted by the LDRW model and the FPT model in order to estimate the MTT of the contrast between the first and the second ROI.

The volume V between the two detection sites (before and after the tube network in Fig. 5), is estimated as given in (13), where the MTT difference (ΔMTT) between the two measured IDCs is multiplied times the flow Q [29], [30].

$$V = \Delta MTT \cdot Q = \Delta\mu \cdot Q \tag{13}$$

The IDC analysis system is implemented in Labview® (National Instruments, Austin, TX) and Matlab®, (The Mathworks, Natick, MA) and runs on a personal computer. Apart from the off-line acoustic densitometry of digital records, real-time video densitometry of analog video outputs of ultrasound scanners can also be performed.

The *in vivo* application of the system in humans requires the use of specific cardiac views where more IDCs can be measured simultaneously. A four-chamber view, for instance, allows the measurement of four IDCs, one for each chamber, leading to an easy assessment of pulmonary, central, intrathoracic, and systemic blood volumes.

Fig. 8 shows the application of the system to a real patient. A transthoracic four-chamber view is used for the measurement. The PBV is assessed by placing two ROI in the right ventricle and left atrium. The bolus (0.25 mg of SonoVue in 5 mL of saline) is injected into a peripheral vein (arm). The CO is assessed by aortic Doppler time-integration technique.

III. Results

The hydrodynamic system described in Fig. 5 is used to measure different volumes. The volume of the tube network is changed by clamping the tubes in specific sites.

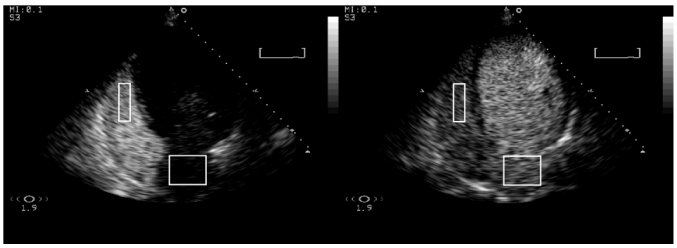

Fig. 8. Transthoracic four-chamber view of the heart after a peripheral injection of a 0.25-mg bolus of SonoVue. On the left, the opacification of the right side of the heart is shown, while later, on the right, the left side of the heart is opacificated. Two ROI are placed in the right ventricle and the left atrium for the IDC measurements.

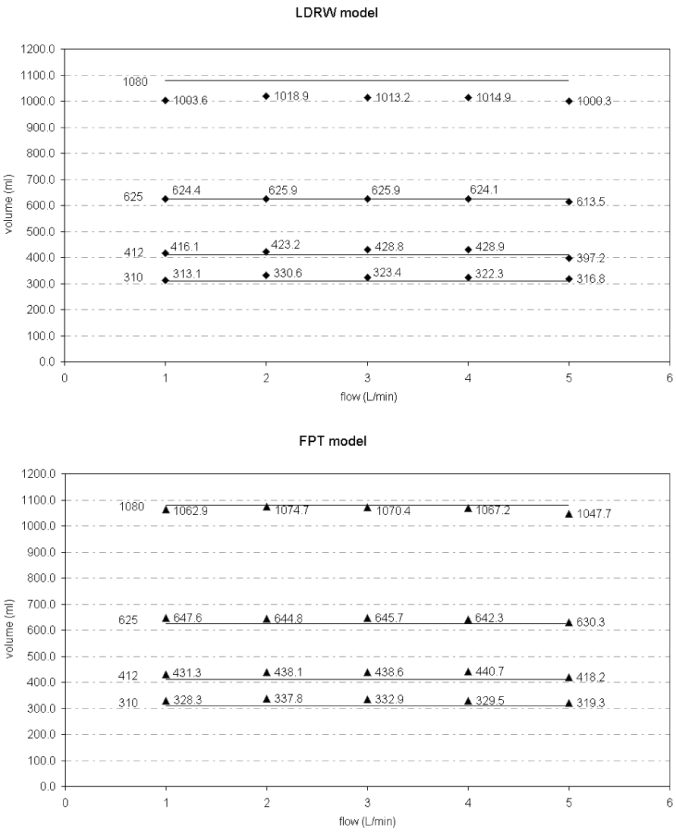

Fig. 9. *In vitro* flow measurements for different flows using the LDRW (upper) and the FPT (lower) model fits.

Four different volumes are defined: 310, 412, 625, and 1080 mL. The volumes are measured for five different flows, from 1 L/min to 5 L/min. Both the LDRW and the FPT models are used for the IDC fitting [see (1) and (2)]. The flow is measured by the electromagnetic flowmeter that is combined with the pump (see Fig. 5). The resulting volume estimates are plotted in Fig. 9 for both the LDRW and the FPT model fits.

The percent standard deviation of the measurements with respect to the average estimate (from the small to the large volume) is 2.1, 3.2, 0.8, and 0.7% for the LDRW fits, and 2.2, 2.2, 1.1, and 1% for the FPT model fits. Fig. 10 shows the average estimates over all five flows using both

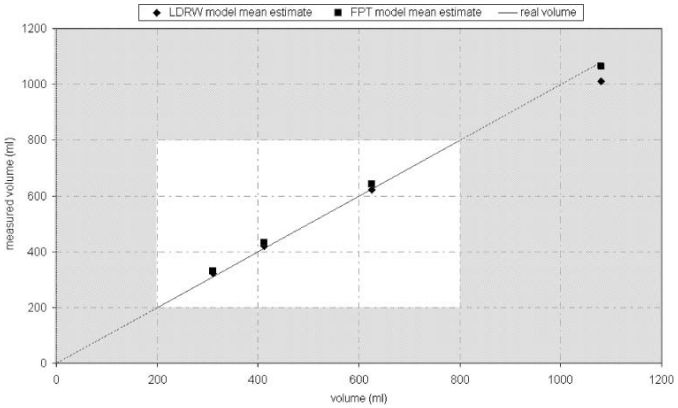

Fig. 10. Average volume estimates over five different flows using both the LDRW and the FPT model fits. The line indicates the real volume. In the middle of the plot, the expected physiological range is highlighted.

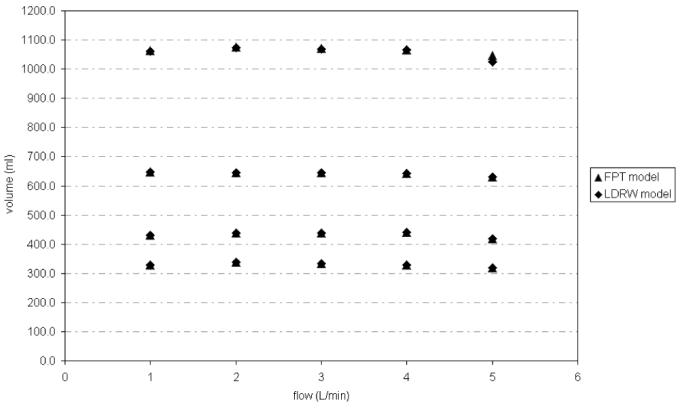

Fig. 11. Volume measurements by FPT model MTT estimates and LDRW model MRT estimates.

models. The physiologic range for PBV measurements is highlighted[4] [7], [8]. The determination coefficient between the real and the estimated volumes is larger than 0.999 for both the LDRW and the FPT model fits.

Both approaches produce very stable results in a wide range of flows. However, the FPT model volume estimates show an average overestimation of 3.2% with respect to the LDRW model estimates, which are very accurate in the physiological PBV range. This is explained by the single-passage hypothesis of the FPT model. In fact, since both models show excellent IDC fits (determination coefficient larger than 0.9), the estimates for the parameter μ as derived from the FPT model are very close to the MRT estimates from the LDRW model (Fig. 11). As a consequence, the overestimation is quantified by the term μ/λ from the LDRW model, which is related to the diffusion-to-convection ratio. When the diffusion component is larger, the difference between MTT and MRT is more pronounced.

[4]The provided PBV values are non-indexed, i.e., they are not divided by the body surface area index.

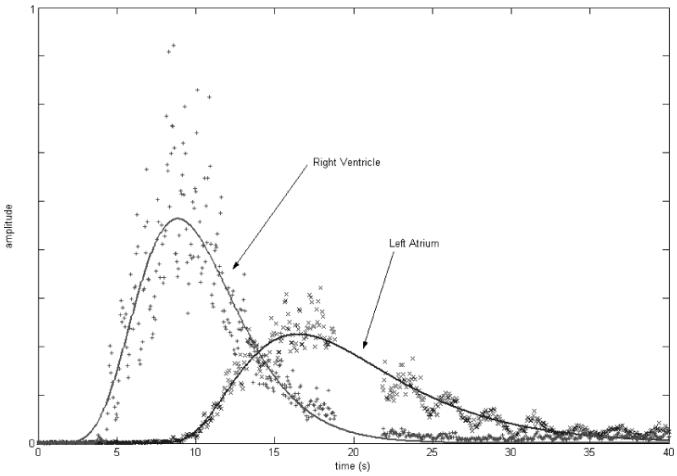

Fig. 12. LDRW fits of two IDCs recorded from the right ventricle and the left atrium of a patient after an injection of 0.25 mg of SonoVue diluted in 5 mL of saline.

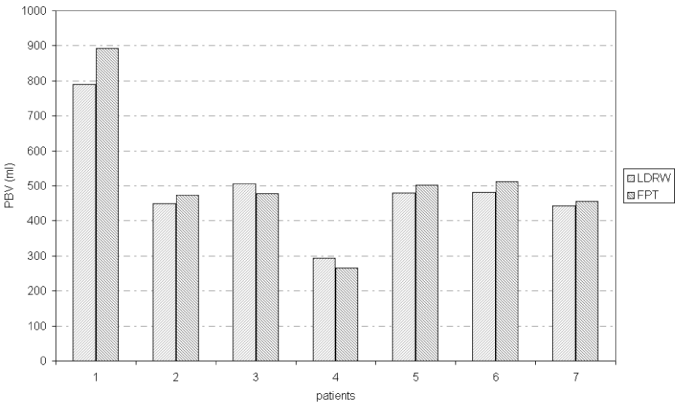

Fig. 13. PBV measurements in patients. Both the LDRW and the FPT model estimates are shown.

The physical interpretation for the MTT-MRT difference in the UCA dilution context stands in the low MI insonation. The adopted 0.1 MI does not produce a significant bubble disruption rate. As a consequence, the FPT model hypothesis is not realistic.

Due to a problem in the volume network, the flow in the two main brunches of the largest volume (1080 mL) was unbalanced. As a consequence, the resulting IDC is the sum of two different IDCs with different MTT. The fit of such a curve, as confirmed by specific simulation, provides with a MTT estimate that is close to the smallest MTT. This might be the reason for the underestimation of the largest volume with both models. However, a volume of 1080 mL is beyond the physiological boundaries for the PBV.

The system was also tested in humans. Fig. 8 shows a transthoracic four-chamber view, which was used to select two ROI in the right ventricle and the left atrium. The right ventricle and left atrium IDCs were measured and fitted by the models (Fig. 12). CO was assessed by aortic time-integration echo-Doppler. The ΔMTT were estimated from the IDC and multiplied times CO to obtain the PBV estimates. Fig. 13 shows the measured PBV in a group of seven patients.

Except for the first patient, the difference between LDRW and FPT model estimates was minimal. In fact, the cardiac valves reduced the number of bubble passages through the detection sites (cardiac chambers) and the difference between MTT and MRT was minimal. All the patients who showed a large PBV are heart failure patients (candidate for bioventricular pacing). The only patient who showed a small PBV (number 4 in Fig. 13) has a normal heart and is a candidate for pneumonectomy. These preliminary results correspond to the expectations. In fact, a decrease of left ventricular efficiency could be compensated by a pulmonary blood volume (and pressure) increase.

With respect to classic transpulmonary techniques [8], we are able to exclude the right atrium, left ventricle, and aortic volume from the PBV measurement, resulting in a more accurate estimate.

IV. Discussion and Conclusions

The assessment of blood volumes in the circulatory system provides valuable information for both diagnosis and patient monitoring. Unfortunately, such measurements used to be difficult to obtain and required the use of invasive techniques. These measurements were not an ambulatory procedure and required hospitalization.

The use of contrast echocardiography overcomes the invasiveness issue, so that pulmonary, central, intrathoracic, systemic, and other blood volume assessments can become a standard procedure in outpatients.

A bolus of UCA is injected into a peripheral vein and detected by a transthoracic ultrasound transducer for the simultaneous IDC measurement from different sites in the central circulation. Blood volumes between different detection sites are calculated as the product between blood flow and contrast MTT, which are derived from the LDRW or the FPT fit of the IDCs. Blood flow measurements can be performed by any non-invasive technique (e.g., aortic echo-Doppler).

The method was validated *in vitro*. The results show stable and reproducible volume estimates for a wide range of flows. In general, the LDRW model volume estimates are more accurate. Especially when the diffusion component is more pronounced, the FPT model estimates show a bias (overestimation) that is a consequence of the single-passage hypothesis. Such an assumption is unrealistic in the UCA dilution context. In fact, due to the low MI, only a minimal fraction of bubbles are destroyed while passing through the ultrasound beam.

The system was also tested in humans with very promising results. The difference between LDRW and FPT volume estimates in patients was minimal. This is a consequence of the cardiac valves, which reduce the number of bubble passages through the detection ROI.

In conclusion, the blood volume assessment by use of UCA dilution is feasible and accurate. The measurement

can be performed with minimal invasiveness. As a consequence, this technique may be a real asset in cardiology, anesthesiology, and intensive care, since it allows the measurement of important diagnostic clinical parameters that cannot be measured without the use of very invasive techniques. Physiological processes can be studied in more detail resulting in increased knowledge, for instance, of the time course of chronic heart failure patients with minimal risk and discomfort for the patient and, possibly, new therapeutic strategies.

Moreover, this technique opens new possibilities for studying the relation between blood volumes and cardiac diseases. The characterization of this relation as well as a more extensive *in vivo* validation will be the object of future study. Further research will also concern the use of the recirculation curve fit (see Fig. 2) in order to assess the total circulating blood volume, which could be used to normalize the value of the other partial volumes.

Appendix A

The derivation of the FPT model is rather complicated. However, it can be simplified by exploiting the LDRW model definition. The probability $p(x,t)$ that a bubble moves from a distance $d = 0$ to $d = x$ in time t is described by the unbiased (diffusion without drift) LDRW model as given in (14), where D is the diffusion constant.

$$p(x,t) = \frac{1}{\sqrt{4\pi Dt}} e^{-\frac{x^2}{4Dt}} \tag{14}$$

If the bubble reaches the distance x for the first time at time $t-\tau$ ($\tau \in [0,t]$), the probability of finding the particle at distance x at time t can be divided into two contributions: $l(x,t-\tau)$ and $p(0,\tau)$. The $l(x,t-\tau)$ term is the probability of a first passage in x at time $t-\tau$, and $p(0,\tau)$ is the probability of a subsequent passage in x at time τ after the first passage. Thus, $p(x,t)$ is given by a convolution operation as in (15).

$$p(x,t) = \int_0^t l(x,t-\tau)p(0,\tau)\cdot d\tau \tag{15}$$

In the Laplace domain, (15) can be expressed as given in (16).

$$P(x,s) = L(x,s)\cdot P(0,s) \tag{16}$$

As a consequence, $L(x,s)$ is given as in (17).

$$L(x,s) = \frac{P(x,s)}{P(0,s)} \tag{17}$$

The $p(x,t)$ term is expressed in the Laplace domain as given in (18).

$$P(x,s) = \frac{1}{\sqrt{4\pi Ds}} e^{-\sqrt{\frac{x^2 s}{D}}} \tag{18}$$

Therefore, $L(x,s)$ is given as in (19).

$$L(x,s) = e^{-\sqrt{\frac{x^2 s}{D}}} \tag{19}$$

The FPT process is the anti-transformation in the time domain of $L(x,s)$, which is given as in (20).

$$l(x,t) = \frac{x}{\sqrt{4\pi Dt^3}} e^{-\frac{x^2}{4Dt}} \tag{20}$$

The $l(x,t)$ term represents the probability density function that the bubble reaches the distance x for the first time at time t.

The same procedure is applicable in case of drifting diffusion. The $p(x,t)$ term is now defined as given in (21), where u is the carrier fluid velocity.

$$p(x,t) = \frac{1}{\sqrt{4\pi Dt}} e^{-\frac{(x-ut)^2}{4Dt}} \tag{21}$$

If the detection distance is fixed to $x = x_0 = \mu u$, and $D/u^2 = K^2$, (21) can be rewritten as given in (22).

$$p(\mu,t) = \frac{1}{u\sqrt{4\pi K^2 t}} e^{-\frac{(\mu-t)^2}{4K^2 t}} \tag{22}$$

The model is valid for $u > 0$. For $u = 0$, the diffusion without drift model must be used. As for the diffusion without drift case, (22) is substituted into (15), which is now expressed as given in (23).

$$p(\mu,t) = \int_0^t l(\mu,t-\tau)p(0,\tau)\cdot d\tau \tag{23}$$

Eq. (23) can be solved again in the Laplace domain. The resulting $L(\mu,s)$ represents the FPT model in the Laplace domain when drift is included. The $L(\mu,s)$ term is expressed as given in (24).

$$L(\mu,s) = e^{-\frac{\mu\left(1-\sqrt{1-4sK^2}\right)}{2K^2}} \tag{24}$$

Taking the inverse Laplace transform, (24) is expressed in the time domain as given in (25).

$$l(\mu,t) = \frac{\mu}{\sqrt{4\pi K^2 t^3}} e^{-\frac{(\mu-t)^2}{4K^2 t}} \tag{25}$$

The $l(\mu,t)$ term represents the FPT model with drift in the time domain. Since $L(\mu,0) = 1$, the integral of $l(\mu,t)$ in the interval $(0,\infty)$ equals 1 and $l(\mu,t)$ may be considered as a statistical distribution. With the substitution $\lambda = (u\mu)/(2D)$, (25) is expressed as given in (2), which is the FPT model definition as reported by Bogaard *et al.* [25]–[27]. The first moment of the model, as proven by Sheppard [4], is equal to μ.

Acknowledgment

The authors thank the Department of Cardiology of the Catharina Hospital Eindhoven and, in particular, Annemieke Jansen for supplying this study with the contrast echographies in patients. The authors also thank the perfusionists and the operating room staff of the Catharina Hospital Eindhoven, and, in particular, Susan van den Elzen for her valuable support with the *in vitro* experimentation.

References

[1] A. J. G. H. Bindels, J. G. van der Hoeven, A. D. Graafland, J. de Koning, and A. E. Meinders, "Relationships between volume and pressure measurements and stroke volume in critically ill patients," *Crit. Care*, vol. 4, pp. 193–199, 2000.

[2] A. Hoeft, B. Schorn, A. Weyland, M. Scholz, W. Buhre, E. Stepanek, S. J. Allen, and H. Sonntag, "Bedside assessment of intravascular volume status in patients undergoing coronary bypass surgery," *Anesthesiology*, vol. 81, pp. 76–86, 1994.

[3] K. H. Norwich, *Molecular Dynamics in Biosystems*. New York: Pergamon Press, 1977.

[4] C. W. Sheppard, *Basic Principles of Tracer Methods: Introduction to Mathematical Tracer Kinetics*. New York: Wiley, 1962.

[5] K. Zierler, "Indicator dilution methods for measuring blood flow, volume, and other properties of biological systems: A brief history and memoir," *Ann. Biomed. Eng.*, vol. 28, pp. 836–848, 2000.

[6] S. G. Sakka, C. C. Ruhl, U. J. Pfeiffer, R. Beale, A. McLuckie, K. Reinhart, and A. Meier-Hellmann, "Assessment of cardiac preload and extravascular lung water by single transpulmonary thermodilution," *Intensive Care Med.*, vol. 26, pp. 180–187, 2000.

[7] W. Buhre, S. Kazmaier, H. Sonntag, and A. Weiland, "Changes in cardiac output and intrathoracic blood volume: A mathematical coupling of data?," *Acta Anaesthesiol. Scand.*, vol. 45, pp. 863–867, 2001.

[8] W. Buhre, A. Weyland, K. Buhre, S. Kazmaier, K. Mursch, M. Schmidt, M. Sydow, and H. Sonntag, "Effects of the sitting position on the distribution of blood volume in patients undergoing neurosurgical procedures," *Br. J. Anaesth.*, vol. 84, no. 3, pp. 354–357, 2000.

[9] O. Picker, G. Weitasch, T. W. L. Sceeren, and J. O. Arnd, "Determination of total blood volume by indicator dilution: A comparison of mean transit time and mass conservation principle," *Intensive Care Med.*, vol. 27, pp. 767–774, 2001.

[10] L. A. Geddes, "Cardiac output measurement," in *The Biomedical Engineering Handbook*. 2nd ed. J. D. Bronzino, Ed. Boca Raton, FL: CRC Press, 2000.

[11] H. Becher and P. N. Burns, *Handbook of Contrast Echocardiography*. Heidelberg: Springer, 2000.

[12] B. Herman, S. Einav, and Z. Vered, "Feasibility of mitral flow assessment by echo-contrast ultrasound, Part I: Determination of the properties of echo-contrast agents," *Ultrasound Med. Biol.*, vol. 26, no. 5, pp. 785–795, 2000.

[13] P. J. A. Frinking and N. de Jong, "Modeling of ultrasound contrast agents," in *Proc. IEEE Ultrason. Symp.*, 1997, pp. 1601–1604.

[14] A. Bouakaz, N. de Jong, L. Gerfault, and C. Cachard, "In vitro standard acoustic parameters of ultrasound contrast agents: Definitions and calculations," in *Proc. IEEE Ultrason. Symp.*, vol. 2, 1996, pp. 1445–1448.

[15] A. Bouakaz, N. de Jong, and C. Cachard, "Standard properties of ultrasound contrast agents," *Ultrasound Med. Biol.*, vol. 24, no. 3, pp. 469–472, 1998.

[16] N. Sponheim, L. Hoff, A. Waaler, B. Muan, H. Morris, S. Holm, M. Myrum, N. de Jong, and T. Skotland, "Albunex—a new ultrasound contrast agent," *IEEE Conf. Acoust. Sens. Imag.*, vol. 369, pp. 103–107, Mar. 29–30, 1993.

[17] V. Uhlendorf, "Physics of ultrasound contrast imaging: Scattering in the linear range," *IEEE Trans. Ultrason., Ferroelect., Freq. Contr.*, vol. 41, no. 1, pp. 70–79, Jan. 1994.

[18] J. M. Gorce, M. Arditi, and M. Schneider, "Influence of bubble size distribution on echogenecity of ultrasound contrast agents: A study of SonoVue," *Invest. Radiol.*, vol. 35, no. 11, pp. 661–671, 2000.

[19] W. R. Hedrick, D. L. Hykes, and D. E. Starchman, *Ultrasound Physics and Instrumentation*. 3rd ed. New York: Mosby, 1995.

[20] M. Shneider, "Characteristics of SonoVue," *Echocardiography*, vol. 16, no. 7, pt. 2, pp. 743–746, 1999.

[21] C. S. Sehgal and P. H. Arger, "Mathematical modeling of dilution curves for ultrasonographic contrast," *J. Ultrasound Med.*, vol. 16, pp. 471–479, 1997.

[22] M. Mischi, A. A. C. M. Kalker, and H. H. M. Korsten, "Videodensitometric methods for cardiac output measurements," *EURASIP J. Appl. Signal Processing*, vol. 2003, no. 5, pp. 479–489, 2003.

[23] C. W. Sheppard and L. J. Savage, "The random walk problem in relation to the physiology of circulatory mixing," *Phys. Rev.*, vol. 83, pp. 489–490, 1951.

[24] M. E. Wise, "Tracer dilution curves in cardiology and random walk and lognormal distributions," *Acta Phisiol. Pharmacol. Neerl.*, vol. 14, pp. 175–204, 1966.

[25] J. M. Bogaard, S. J. Smith, A. Versprille, M. E. Wise, and F. Hagemeijer, "Physiological interpretation of skewness of indicator-dilution curves; Theoretical considerations and practical application," *Basic Res. Cardiol.*, vol. 79, pp. 479–493, 1984.

[26] J. M. Bogaard, J. R. C. Jansen, E. A. von Reth, A. Versprille, and M. E. Wise, "Random walk type models for indicator-dilution studies: Comparison of a local density random walk and a first passage times distribution," *Cardiovasc. Res.*, vol. 20, no. 11, pp. 789–796, 1986.

[27] E. A. Reth and J. M. Bogaard, "Comparison of a two-compartment model and distributed models for indicator dilution studies," *Med. Biol. Eng. Comput.*, vol. 21, pp. 453–459, 1983.

[28] R. K. Millard, "Indicator-dilution dispersion models and cardiac output computing methods," *Am. J. Physiol.-Heart Circ. Physiol.*, vol. 272, no. 4, pt. 2, pp. H2004–H2012, Apr. 1997.

[29] M. Mischi, A. A. C. M. Kalker, and H. H. M. Korsten, "Blood volume measurements by videodensitometric analysis of ultrasound-contrast-agent dilution curves," in *IEEE-EMBS Proc. 25th Annu. Int. Conf. IEEE Eng. Med. Biol. Soc.*, Sep. 17–21, 2003, pp. 971–974.

[30] M. Mischi, A. H. M. Jansen, A. A. C. M. Kalker, and H. H. M. Korsten, "Intra-thoracic blood volume assessment by dilution of ultrasound contrast agents," in *IEEE-UFFC Proc. IEEE Int. Ultrason. Symp.*, Oct. 5–8, 2003, pp. 1179–1182.

[31] H. Feigenbaum, *Echocardiography*. 5th ed. Philadelphia: Lea & Febiger, 1994.

[32] P. Ask and P. Ake Oberg, "Blood flow measurements," in *Measurement, Instrumentation, and Sensor Handbook*. J. G. Webster, Ed. Boca Raton, FL: CRC Press, 2000.

[33] P. A. Jansson, *Deconvolution with Applications in Spectroscopy*. London: Academic Press, 1984.

[34] P. A. Jansson, *Deconvolution of Images and Spectra*. London: Academic Press, 1997.

[35] A. Papoulis, *Signal Analysis*. New York: McGraw-Hill, 1984, pp. 337–348.

[36] P. Z. Peebles, *Probability, Random Variables, and Random Signal Principles*. 3rd ed. New York: McGraw-Hill, 1993, pp. 303–307.

Massimo Mischi was born in Rome (Italy) in 1973. In 1999, he received his M.S. degree in electronic engineering at La Sapienza University of Rome. In his final thesis he designed and validated a new device for optical-performance measurements of clinical fiber-optic endoscopes. In 2002, he completed a two-year post-Master program in Technological Design, Information and Communication Technology at the Eindhoven University of Technology (The Netherlands) studying the application of indicator dilution theory and

ultrasound contrast agents for cardiac output measurements. Currently he is a Ph.D. candidate and a research assistant at the Eindhoven University of Technology. His research concerns the quantification of cardiac parameters by means of contrast echocardiography. Mr. Mischi is a student member of IEEE. He is also registered in the Italian Public Register of Engineers and in the Dutch Royal Institute of Engineers.

Ton A. Kalker (M'93–SM'99–F'02) was born in The Netherlands in 1956. He received his M.S. degree in mathematics in 1979 from the University of Leiden, The Netherlands. From 1979 until 1983, while he was a Ph.D. candidate, he worked as a research assistant at the University of Leiden. From 1983 until December 1985, he worked as a lecturer at the Computer Science Department of the Technical University of Delft. In January 1986, he received his Ph.D. degree in Mathematics. In December 1985, he joined the Philips Research Laboratories, Eindhoven. Until January 1990, he worked in the field of computer-aided design. He specialized in (semi-)automatic tools for system verification. Currently he is a member of the Digital Signal Processing group of Philips Research. His research interests include wavelets, multirate signal processing, motion estimation, psycho-physics, digital video compression, medical imaging, digital watermarking, and multimedia security. Dr. Kalker is a Fellow of the IEEE.

Erik H. Korsten was born in the Netherlands in 1953. He studied medicine at Groningen University, Groningen, The Netherlands, and graduated as a medical doctor in 1978. During his training as an anesthesiologist in Utrecht, he started his Ph.D. study on the measurement of intrathoracic fluid content during open-heart surgery. In November 1984, he received his Ph.D. degree in medicine from the University of Leiden, The Netherlands. From June 1982 until the present, he has been a staff member of the Department of Anesthesiology, Intensive Care and Pain Treatments in the Catharina Hospital, Eindhoven. From 1989 until 1993 he was the chairman of the professional medical staff of this hospital (a large teaching hospital in the south of the Netherlands). He is also an intensivist and was head of the Intensive Care Unit during the period 1993 until 2001. During this period he was one of the initiators of a national intensive care database. He was also involved in research projects on data storage and data mining of patient data, as well as the development of artificial intelligence in intensive care. In 2001, he was appointed professor at the Department of Electrical Engineering, Eindhoven University of Technology, The Netherlands.